

Experimental Measurement of Ion Toroidal Rotation in an FRC with RMF Current Drive

A. M. Peter, E. A. Crawford (University of Washington)

Abstract

An important consideration for RMF current drive is that the applied RMF torque does not simply spin the plasma. If the RMF frequency is sufficiently higher than the ion cyclotron frequency, then the ions will not be directly spun up by the RMF but will still experience a frictional drag force applied by the electrons. In the absence of any retarding force, the ions will spin up in a time $\tau = (m_i/m_e)v_{\perp}^{-1}$. Because of the elevated resistivity in TCS ($\eta_{\perp} \sim 100 \mu\Omega\text{-m}$ and $v_{\perp} \sim 5 \times 10^7 \text{ s}^{-1}$), this time is quite short ($\sim 75 \mu\text{s}$). This rapid spin-up has not been observed experimentally, however. To measure ion rotation, the TCS device has been equipped with an intensified CCD spectrometer. C-III emission at 229.7 nm is viewed at six chords, allowing determination of a rotation profile through Abel inversion. Impurity ions are observed to only spin up to a small fraction of the electron velocity (3% at $\omega_{\text{RMF}} = 1 \times 10^6 \text{ s}^{-1}$, 15% at $\omega_{\text{RMF}} = 0.5 \times 10^6 \text{ s}^{-1}$) and the toroidal current is maintained in steady state. The primary braking mechanism on the ions may be charge-exchange with a background of cold, stationary neutrals. The inferred charge-exchange rate requires a neutral density equal or greater than the plasma density. This neutral density is higher than that suggested by power balance, so additional braking mechanisms may be acting on the ions.

Introduction

A rotating magnetic field (RMF) can inductively drive toroidal current in an FRC, sustaining the poloidal flux. If $\omega_{\text{RMF}} \gg \omega_{\text{ci}}$, then the RMF does not put any toroidal force directly on the ions. However, the RMF is exerting a real torque on the plasma. The electron current will eventually spin up the ions in the ion paramagnetic direction through collisions. To study the dynamics of this process, the TCS device has been equipped with a multi-chord intensified CCD spectrometer to measure ion rotation profiles.

Description of Diagnostic

The TCS ICCD spectrometer is an Acton Research SpectraPro 500i Czerny-Turney with a focal length of 0.5 m and an aperture ratio of f/6.5. Toroidal optics provide the necessary spectral resolution while allowing sufficient vertical resolution to image six fibers simultaneously. Two gratings are used, one with a blaze wavelength of 500 nm and a holographic grating with a blaze of 250 nm. Both have 1800 g/mm, yielding a nominal dispersion of 0.9 nm/mm, which corresponds to 0.22 angstroms per pixel on the CCD.

The ICCD array is contained in a Princeton Instruments PI-MAX 512RB camera. The intensifier contains an 18-mm Gen-II photocathode and a micro-channel plate. The gate time for the photocathode voltage is very fast, nominally 2ns, allowing for precise timing of the exposure. The rear phosphor is a type P43 with a decay time of 3 ms, so

only one exposure can be taken per plasma shot. The CCD is a Thomson 7895 square array with 512 x 512 pixels, cooled to -20 deg C to minimize dark current. The data is digitized and read out through an ST-133 controller and A/D converter. The data is then analyzed using IDL and MATLAB.

Six 12-mm quartz plano-convex lenses collect light from the plasma. Each lens focuses light onto a fiber optic bundle, consisting of a hex-close-packed bundle of 200- μm silica fibers. The six fiber bundles can be configured either in a symmetric fan or an asymmetric fan for Abel inversion, as shown in Fig. 1. Impurity line radiation from C-III (229.7 nm) and Si-III (455.3 nm) is typically monitored.

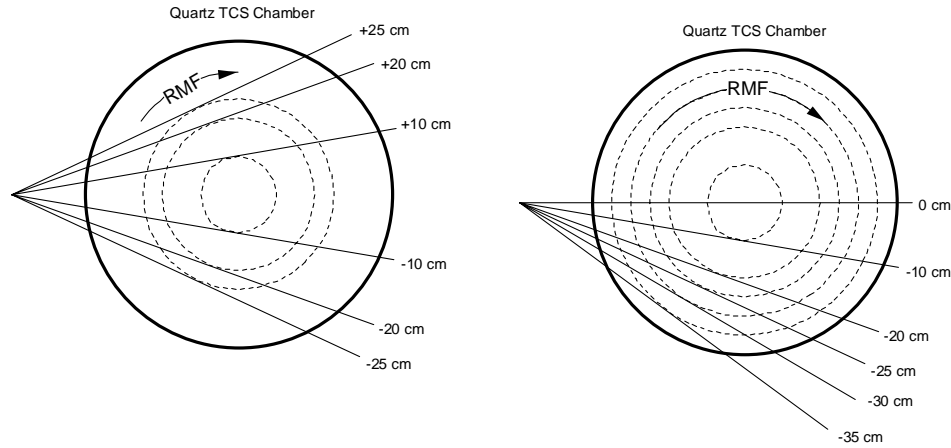


Figure 1. Fiber optic layouts on the TCS device

Data Analysis

Before the CCD data can be binned and analyzed, the curvature due to the toroidal optics must be removed. Correction curves are generated from Hg reference lines. Once the image is “straightened”, the rows corresponding to each fiber are binned. The wavelength center of each spectrum is determined from the centroid:

$$\bar{\lambda} = \frac{\int \lambda f(\lambda) w(\lambda) d\lambda}{\int f(\lambda) w(\lambda) d\lambda}, \quad \text{where } w(\lambda) = 1 - \frac{1}{2} \left| \frac{\lambda - \bar{\lambda}}{\delta} \right|$$

where δ is the half-width-half-maximum. The shift in centroid wavelength from the natural wavelength λ_0 gives a line-of-sight velocity from the Doppler shift equation $\Delta\lambda/\lambda_0 = (v/c) \cos\theta$.

For more detailed rotation profiles, an Abel inversion is performed. The plasma is divided into six shells, each with an inner radius equal to the fiber impact parameter. The plasma emission, rotation frequency, and ion temperature are assumed constant in each shell. The plasma emission in shell j is then inverted from the chord-integrated data for fiber i using a matrix inversion $E_j = \sum_i L_{ij}^{-1} B_i$ where L_{ij} is the length of fiber i in shell

j. The velocity profiles are then inverted by modeling each shell as a gaussian profile and physically subtracting outer spectra from inner ones. Future Abel inversions will use a more robust matrix algorithm that does not depend on gaussian fitting.

Results

Line-of-sight results are shown in Fig. 2. These results are obtained with the symmetric fan as shown in Fig. 1. and are not Abel-inverted.

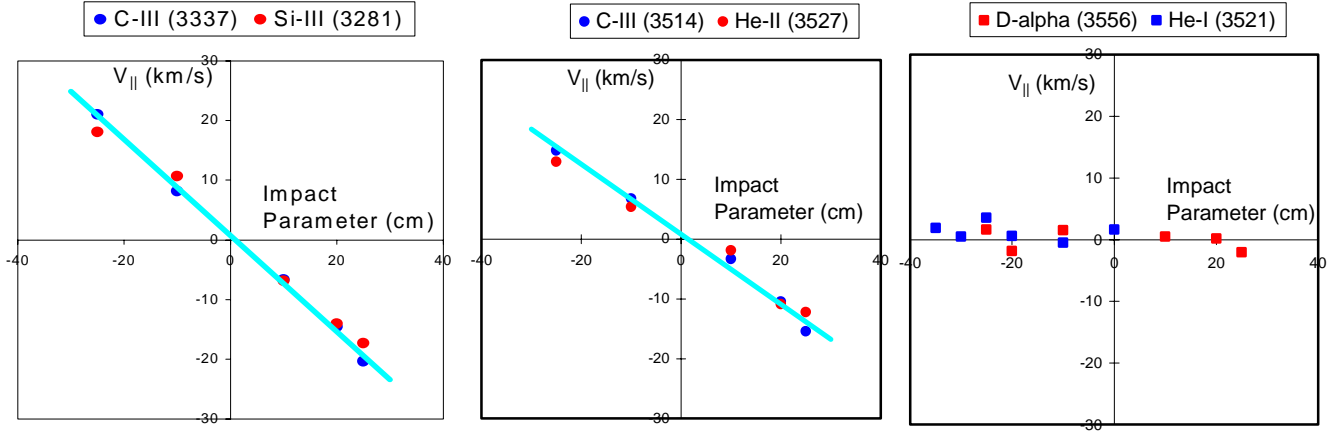


Figure 2. Line-of-sight rotation measurements for various ion and neutral species.

Although line-of-sight results do not allow determination of a rotation profile, they are useful to verify that the plasma is indeed rotating in the ion paramagnetic direction. Furthermore, comparing carbon with silicon and helium provides promising evidence that the impurities are synchronous with the bulk plasma. Neutral emission from both D- α and He-I are not seen to rotate.

Inverted velocity profiles for carbon and silicon are shown in Fig. 3. These show that the plasma is rotating as a rigid body, allowing determination of an ion rotation frequency ω_i and a rotation fraction $\alpha = \omega_i / \omega_e$, shown in Fig. 4. versus time. A simple analysis assuming that the ion steady-state velocity is a balance between electron collisions and charge-exchange collisions allows a rough estimate of neutral density:

$$\alpha = \frac{v_i \theta}{v_e \theta} = \left(1 + \frac{m_i v_{cx}}{m_e v_{ei}} \right)^{-1}$$

Neutral density shown in Fig. 5 is much higher than neutral density inferred from power balance. Additional mechanisms, such as selective loss of paramagnetic ions, end shorting of the radial electric field, and radial flow may be acting on the plasma ions.

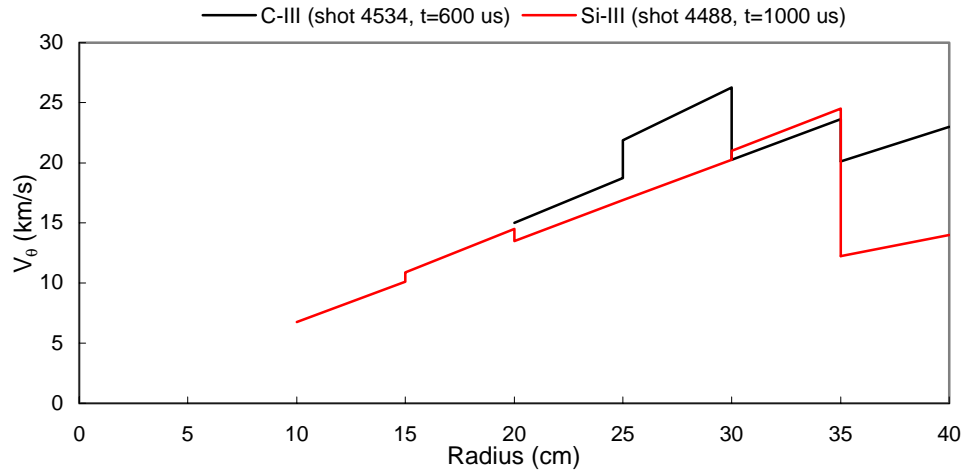


Figure 3: Velocity profiles for carbon and silicon impurities

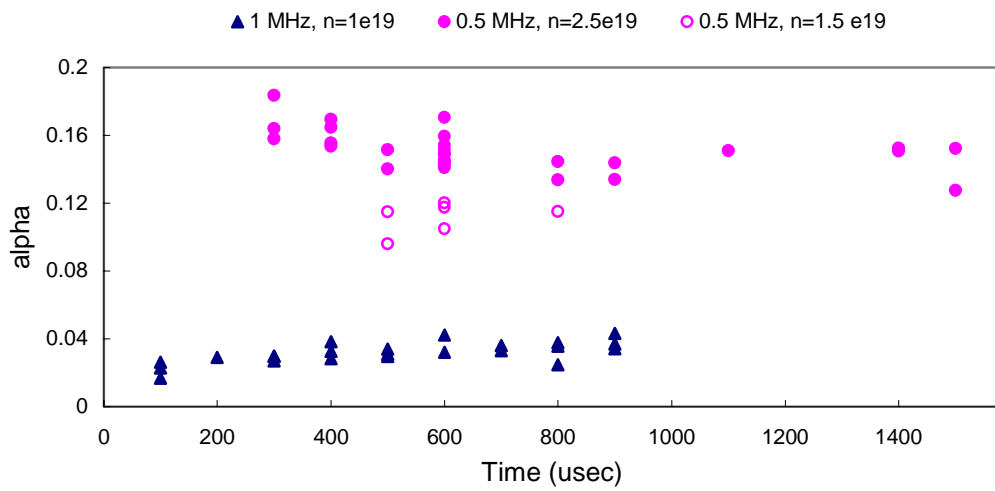


Figure 4: Time evolution of ion rotation fraction (alpha)

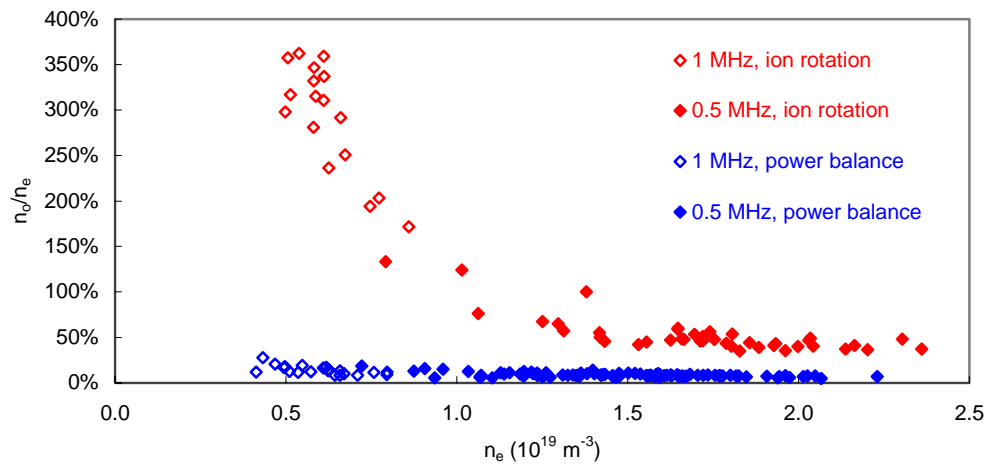


Figure 5: Estimation of neutral density from ion rotation and power balance